GENERATION AND SPATIAL PROPAGATION OF LANDSLIDE GENERATED IMPULSE WAVES

Frederic M. Evers[1] and Willi H. Hager[1]

Large subaerial mass wasting into water may generate large waves along coast lines and in bays. Hazard assessment of such an events is based on the decay rate of these impulse waves along their propagation path to populated areas and infrastructure along the shoreline. The spatial propagation processes of impulse waves generated by deformable slides was investigated in a wave basin. A videometric measurement approach allowed for a detailed tracking of the free water surface and key wave characteristics during the experimental runs including the wave height. Based on selected tests, the slide width effect on spatial wave propagation is discussed.

Keywords: Impulse wave; physical modelling; subaerial landslide; wave height decay; wave propagation

INTRODUCTION

Large subaerial mass wasting events of granular composition such as landslides or rock avalanches may generate large water waves along coast lines and in bays, but also in inland waters. These impulse waves run-up shorelines or overtop dam structures, endangering thereby riparian infrastructure and people. There are numerous accounts of impulse wave events in coastal areas. A rock avalanche in Lituya Bay, USA, generated in 1958 a wave, causing run up heights of more than 500 m a.s.l. (Miller, 1960, Slingerland and Voight, 1979). At Knight Inlet, Canada, an impulse wave presumably destroyed an indigenous settlement in the 16th century (Bornhold et al., 2007). More recent events include Aysén Fjord, Chile, in 2007 (Sepúlveda et al., 2010) and Paatuut, Greenland, in 2000 (Dahl-Jensen et al., 2004). Starting from a limited slide impact zone, the generated wave train propagates omni-directionally across the water body. It is relevant for hazard assessment to understand the processes of spatial impulse wave propagation thereby predicting the rate of wave height decay in particular.

SPATIAL IMPULSE WAVE HEIGHT DECAY

Laboratory experiments allow for the establishment of universal prediction equations for impulse wave hazard assessment. One of the key wave characteristics for predicting wave-shore and wave-structure interactions is the wave height H_1 (Fig. 1a), which is a composite wave characteristic consisting of the wave amplitude a_1 and the following wave trough. Fig. 1a provides an overview of the governing parameters for the description of wave height H_1 at a propagation distance r from the impact location of a granular slide for a two-dimensional test setup (Heller and Hager, 2010). These include slide impact velocity V_s, slide mass m_s, slide thickness s, slide impact angle α, and still water depth h. In a three-dimensional (3D) test setup, the radial propagation distance r is complemented with the wave propagation angle γ and the slide width b (Heller et al., 2009).

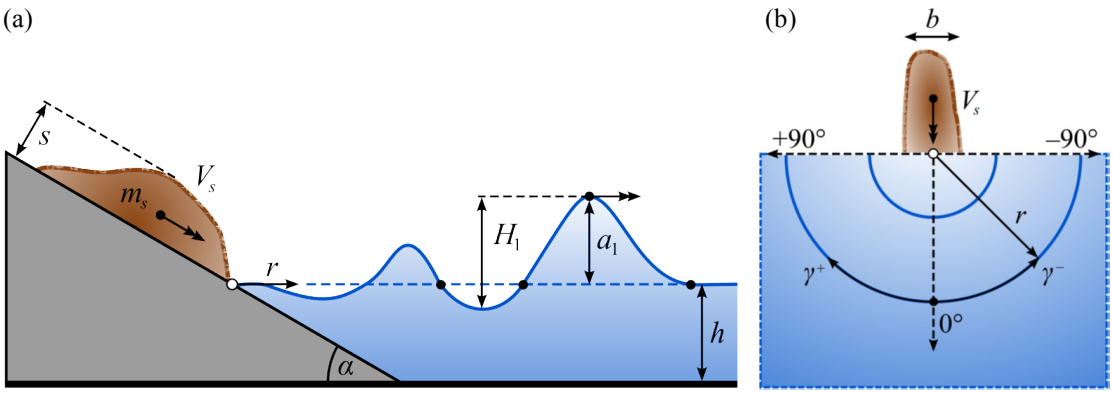

Figure 1. Cross section for γ = 0° (a) and top view (b) of governing parameters and characteristics of first impulse wave crest amplitude and height

[1] Laboratory of Hydraulics, Hydrology and Glaciology (VAW), ETH Zurich, CH-8093 Zürich, Switzerland

Empirical formulations for the decay rate of wave height H_1 were presented by Panizzo et al. (2005), Heller et al. (2009), Mohammed and Fritz (2012), and Heller and Spinneken (2015). Besides discussing the general layout of these equations, Evers and Hager (2016) compare predicted values and measurement data thereby identifying limitations regarding applicability for impulse waves generated by granular slides. The limited applicability arises from either the respective experimental setup, the usage of rigid slide bodies, fixed slide parameters, or the lack of experimental verification. However, Evers and Hager (2016) propose an approach combining the wave generation term of Heller et al. (2009) and the propagation term of and Heller and Spinneken (2015) to satisfactorily predict their measurement data within a scatter range of ±30%. The combined approach includes the impulse product parameter (Heller et al., 2009, Heller and Hager, 2010)

$$\mathsf{P} = \mathsf{F} S^{1/2} M^{1/4} \left\{ \cos\left[\left(6/7 \right) \alpha \right] \right\}^{1/2} \tag{1}$$

This wave generation term includes the slide Froude number $\mathsf{F} = V_s/(gh)^{1/2}$, the relative slide thickness $S = s/h$, the relative slide mass $M = m_s/(\rho_w b h^2)$, and the slide impact angle α. For quantifying wave propagation, the wave decay term $(r/h)^{-1} f_\gamma$ by Heller and Spinneken (2015) was included with

$$f_\gamma = \cos^{2\left\{1+\exp\left[-0.2(r/h)\right]\right\}} \left(2\gamma/3 \right) \tag{2}$$

Introducing f_B as term for the effect of relative slide width $B = b/h$, the combined approach by Evers and Hager (2016) states the relative wave height as

$$Y_1 = H_1/h = \mathsf{P} f_B \left(r/h \right)^{-1} f_\gamma \tag{3}$$

Since their experiments had a fixed relative slide width $B = 2.5$, $f_B = 2$. Eq. (3) is applied in this study for predicting wave heights H_1 generated by granular slides of different widths b.

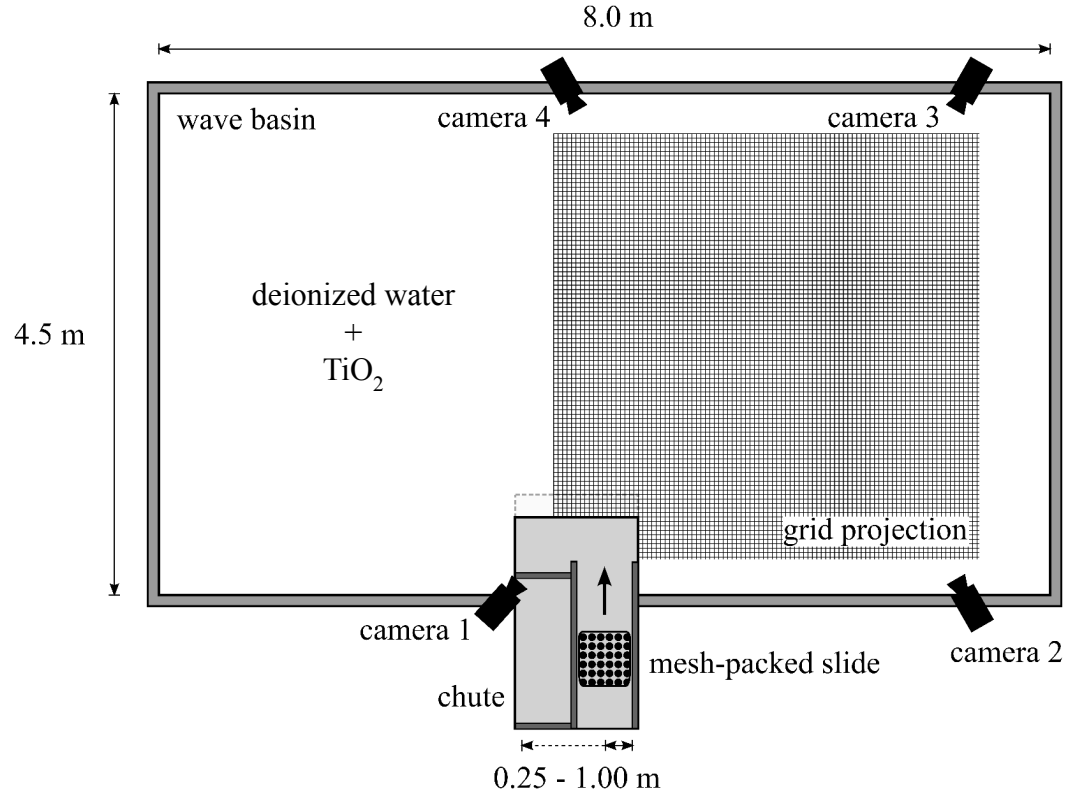

Figure 2. Experimental setup showing positions of the four spatially referenced cameras

EXPERIMENTAL SETUP AND INSTRUMENTATION

The impulse wave experiments were conducted in a rectangular 4.5 m by 8.0 m wave basin (Fig. 2). Wave generation was induced by deformable mesh-packed slides on an inclinable chute. Evers and Hager (2015a) compared this method of wave generation to free granular slides noting an overall agreement regarding wave the characteristics including wave amplitude a_1 and wave height H_1. The geometric dimensions of the sliding mass were predefined in a release box. Besides slide thickness s and different release heights on the sliding plane to vary the slide impact velocity V_s, the release box was adjustable to slide widths b = 0.25, 0.50, and 1.0 m. Transformation of the slide dimensions was found to be negligible during the subaerial acceleration process on the chute. Whereas on slide impact and during underwater slide movement, the mesh-packed slides allowed for deformation as observed for free granular slides. The slide impact velocity V_s was measured with laser light barriers mounted perpendicularly to the sliding plane right above the stillwater surface.

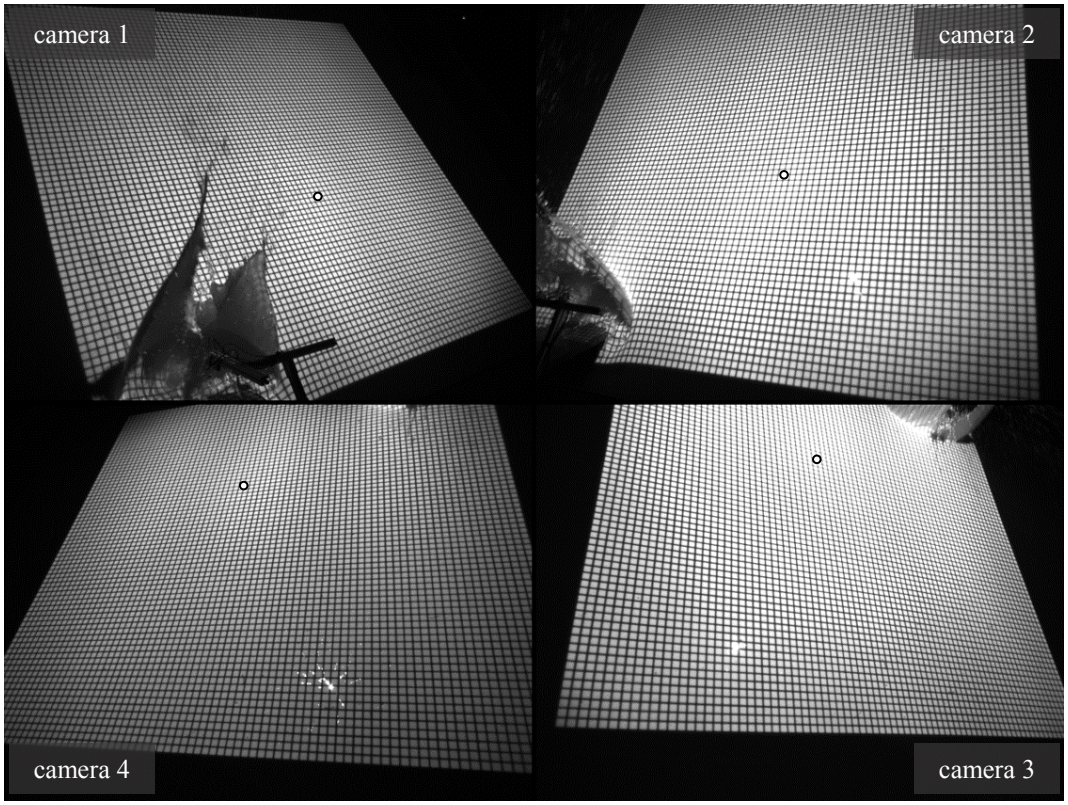

Figure 3. Synchronized multi-camera shot of experimental run; black circles indicate same grid intersection in all four frames

A quasi-continuous representation of the free water surface resulted by applying a videometric measurement system. Four spatially referenced cameras (AICON 3D Systems GmbH, Braunschweig, Germany) record a grid pattern projection on an opaque water surface dyed with titanium dioxide (Figs. 2 and 3). The cameras were operated at a synchronized frame rate of 24 Hz. Fig. 3 shows a synchronized multi-camera shot. The sliding mass has just impacted the water surface generating an impact crater as well as a splash. The black circle illustrates the same grid intersection in all four perspectives. Since the positions and orientations of the four cameras are spatially referenced, this grid intersection is tracked in 3D. The functional principle of the tracking procedure is graphically explained in Fig. 4. Evers and Hager (2015b) provide a comparison between videometrically measured wave profiles and conventional capacitance wave gauges showing satisfactory agreement. This measurement technique allows for tracking up to 6,000 point measurements on a surface area of nearly 14 m^3. Fig. 5 shows the temporal evolution of the first wave crest's spatial propagation pattern for a single experimental run. The high spatial and temporal resolution of the measurement system allows for detailed tracking of the key wave characteristics. Only wave characteristics outgoing from the impact location were investigated, yet measurement data influenced by wave reflection were excluded.

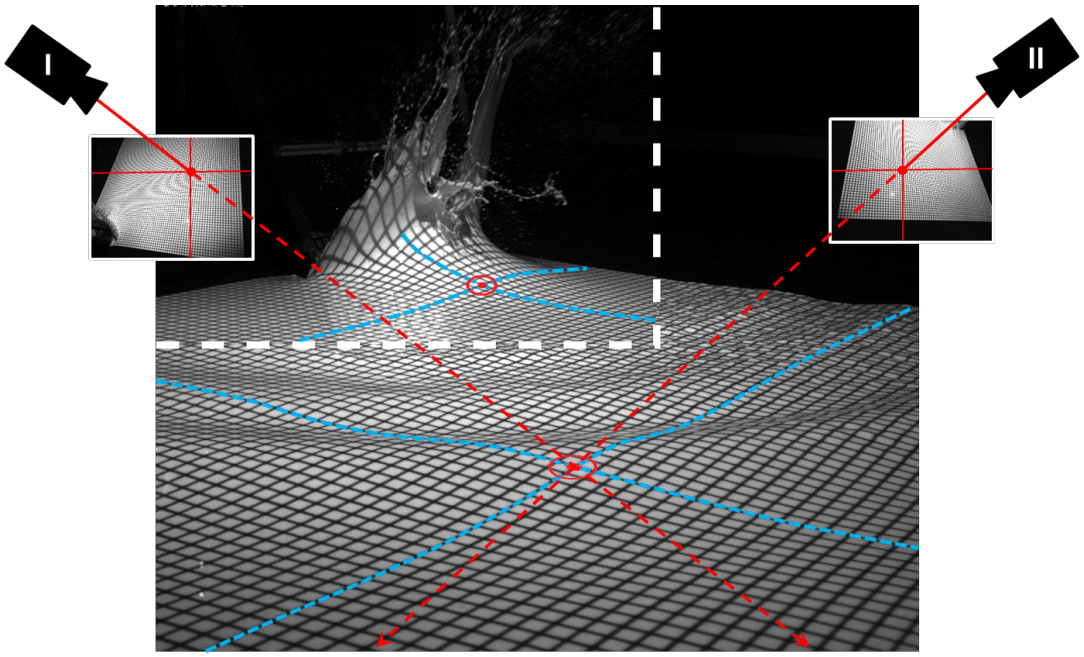

Figure 4. Functional principle of videometric measurement system with two cameras

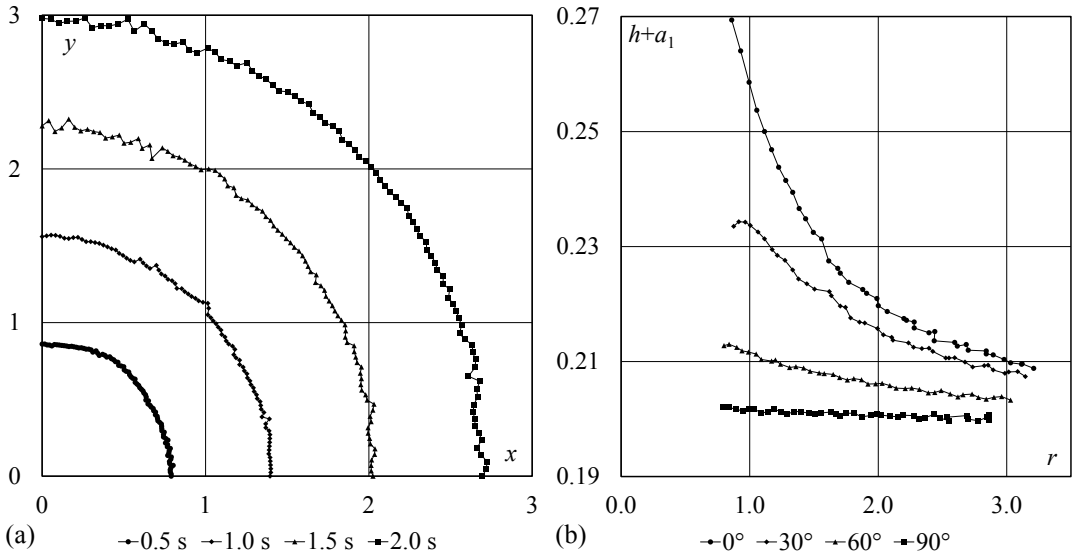

Figure 5. Spatial propagation of first wave crest for t = 0.5, 1.0, 1.5, and 2.0 s (a); and first wave crest amplitude a_1 decay for γ = 0°, 30°, 60°, and 90° (b) at h = 0.2 m

Table 1. Experimental parameters (still water depth h = 0.2 m)

Test	F [-]	S [-]	M [-]	B [-]	α [°]	P [-]
A	1.70	0.3	1.00	1.25	60	0.73
B	1.93	0.3	1.00	2.50	60	0.83
C	1.98	0.3	1.00	5.00	60	0.86

RESULTS AND DISCUSSION

The free water surface contours for four time steps of test B (Tab. 1) are presented in Fig. 6. The continuous contours were interpolated from grid intersections tracked by the videometric measurement system. At t = 0 s in Fig. 6a, the slide has not yet distorted the water surface of stillwater depth h = 0.2 m. The first wave crest has formed at t = 0.5 s in Fig. 6b. The connected blue points mark the location of the first wave amplitude a_1. For propagation angle γ = 0°, a_1 features its maximum extent and is decreasing up to γ = 90°. The connected yellow points mark the initial uplift of the water level due to the approaching wave crest. Its position is crucial for determining reflection effects representing the first distortion of the water surface caused by the outgoing wave train. At t = 1.5 s in Fig. 6c, the wave train also includes the first wave trough (red points/line) and the second wave crest (green points/line). In addition, the connected yellow points in between mark the intersections with the stillwater surface. The first wave crest has partially left the area of the grid projection and its tracking was stopped due to reflection effects at t = 2.5 s in Fig. 6d, while the first wave trough and the second wave crest are still marked. This sequence accounts for the radial propagation pattern of the impulse wave train.

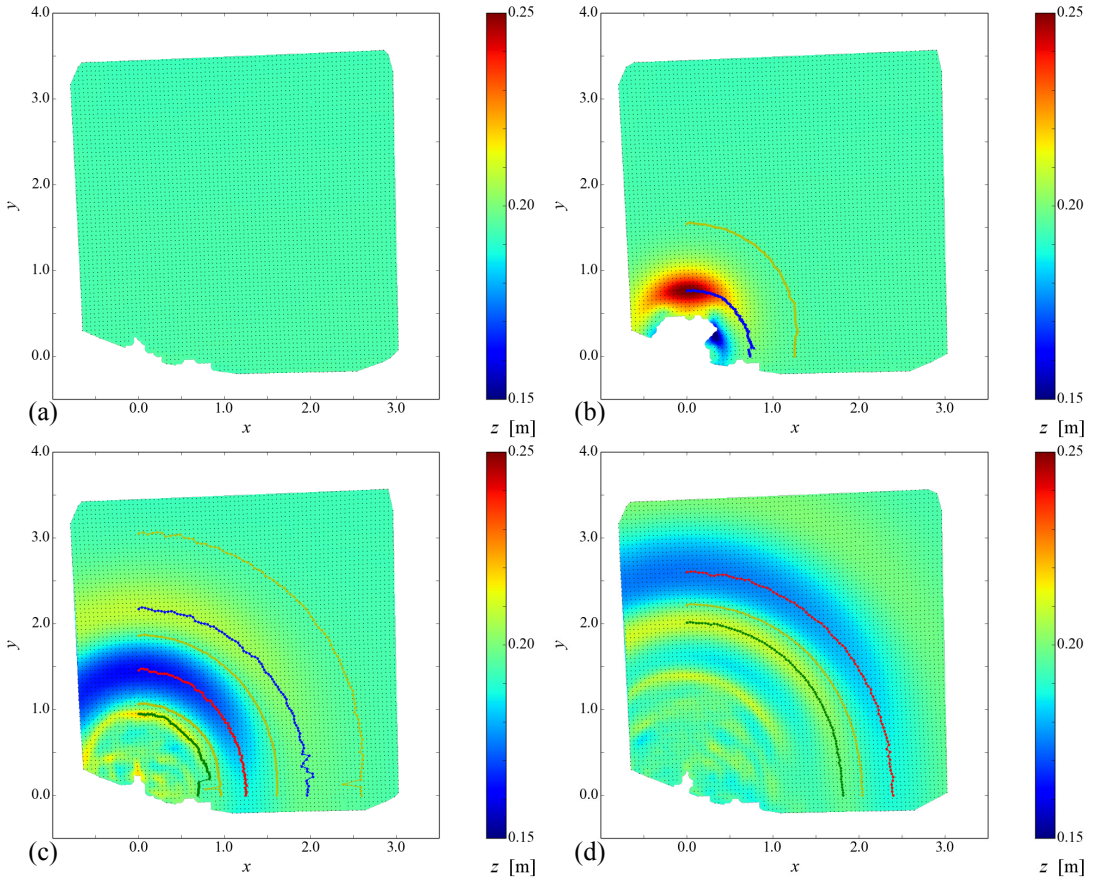

Figure 6. Interpolated free water surface of test B at t = 0.0 s (a), 0.5 s (b), 1.5 (c), and 2.5 s (d) after slide impact; first wave crest (blue line), first wave trough (red line), second wave crest (green line), and stillwater surface intersections (yellow lines)

Three tests are presented for assessing the effect of the slide width b on wave height H_1. The slide parameters of the three tests are specified in Tab. 1. Test A, B, and C feature a slide impact velocity V_s of similar magnitude. Since the relative wave mass M includes the slide width b as denominator, the impulse transferred for wave generation per unit width and thus also the impulse product parameters P share a similar order of magnitude. In 2D test setups where the channel widths correspond to the respective slide widths b, all three test would create wave heights H_1 with only minor deviations among themselves. However, in 3D setups, measured wave heights differ considerably. In the left column of Fig. 7 contour plots are shown for the instant of time when the first wave crest for γ = 0° has propagated to r = 1.0 m. The first wave crest amplitude a_1 at this point increases with increasing slide width b. The

right column of Fig. 7 compares the measured and predicted first wave heights H_1. The prediction results from Eq. (3) by accounting for f_B. As in the experiments by Evers and Hager (2016), the wave heights of test B were predicted with $f_B = 2$. For tests A and C the term was set to $f_B = 1$ and $f_B = 3$, respectively. For test A, $n = 2{,}957$, test B $n = 3{,}295$, and test B $n = 2{,}879$ wave height data points were tracked. While the slide width b was doubled between test A and B and, f_B increased by 100%, doubling of b between test B and C only led to an increase of f_B by 50%. Consequently, the effect of f_B is not linear.

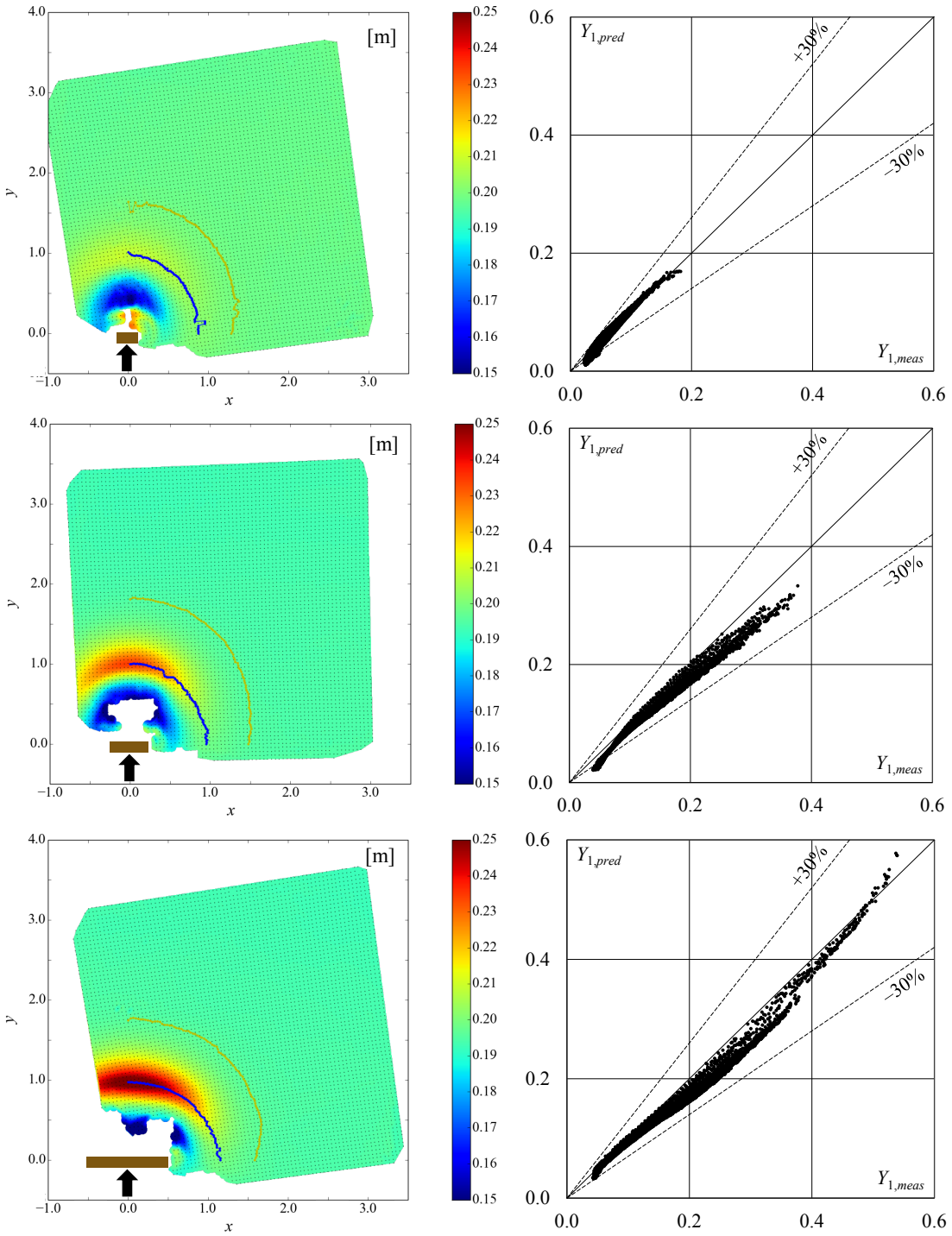

Figure 7. First wave crest contours at $r(\gamma = 0°) = 1.0$ m (left column) and first relative wave height Y_1 measurements vs. predictions (right column) for test A (top), B (middle), and C (bottom)

CONCLUSIONS

Laboratory experiments were conducted in a wave basin for an improved hazard assessment of impulse waves generated by subaerial granular landslides in the spatial environment. A videometric measurement system was applied for tracking the free water surface. This technique allows for a quasi-continuous representation of the outgoing wave train and a detailed analysis of its characteristic including wave amplitudes and heights. The effect of the slide width on wave height generation and propagation was discussed based on selected experiments. An increase of slide width causes an increase of wave height, yet this effect appears to under-proportional.

ACKNOWLEDGMENTS

The first author was funded by the Swiss National Science Foundation (Project No 200021-143657).

REFERENCES

Bornhold, B.D., J.R. Harper, D. McLaren, and R.E. Thomson. 2007. Destruction of the first nations village of Kwalate by a rock avalanche-generated tsunami. *Atmos. Ocean*, 45(2), 123-128. DOI: 10.3137/ao.450205

Dahl-Jensen, T., L.M. Larsen, S.A.S. Pedersen, J. Pedersen, H.F. Jepsen, G.K. Pedersen, T. Nielsen, A.K. Pedersen, F. von Platen-Hallermund, and W. Wenig. 2004. Landslide and tsunami 21 November 2000 in Paatuut, West Greenland. *Natural Hazards*, 31 (1), 277-287. DOI: 10.1023/B:NHAZ.0000020264.70048.95

Evers, F.M., and W.H. Hager. 2015a. Impulse wave generation: Comparison of free granular with mesh-packed slides. *J. Mar. Sci. Eng.*, 3, 100-110. DOI: 10.3390/jmse3010100

Evers, F.M., and W.H. Hager. 2015b. Videometric water surface tracking: towards investigating spatial impulse waves. Proc. 36th *IAHR Congress*, The Hague.

Evers, F.M., and W.H. Hager. 2016. Spatial impulse waves: Wave height decay experiments at laboratory scale. *Landslides*, 13(6), 1395-1403. DOI: 10.1007/s10346-016-0719-1

Heller, V., W.H. Hager, and H.-E. Minor. 2009. Landslide generated impulse waves in reservoirs: Basics and computation. *VAW-Mitteilung* 211, H.-E. Minor, ed. ETH Zurich, Zürich.

Heller, V., and W.H. Hager. 2010. Impulse product parameter in landslide generated impulse waves. *J. Waterway, Port, Coastal, Ocean Eng.*, 136(3), 145–155. DOI: 10.1061/(ASCE)WW.1943-5460.0000037

Heller, V., and J. Spinneken. 2015. On the effect of the water body geometry on landslide–tsunamis: Physical insight from laboratory tests and 2D to 3D wave parameter transformation. *Coast. Eng.*, 104, 113-134. DOI: 10.1016/j.coastaleng.2015.06.006

Miller, D.J. 1960. The Alaska earthquake of July 10, 1958: giant wave in Lituya Bay. *B. Seismol. Soc. Am.* 50(2), 253-266.

Mohammed, F., and H.M. Fritz. 2012. Physical modeling of tsunamis generated by three-dimensional deformable granular landslides. *J. Geophys. Res.*, 117, C11015. DOI: 10.1029/2011JC007850

Panizzo, A., P. De Girolamo, and A. Petaccia. 2005. Forecasting impulse waves generated by subaerial landslides. *J. Geophys. Res.*, 110, C12025. DOI: 10.1029/2004JC002778

Sepúlveda, S.A., A. Serey, M. Lara, A. Pavez, and S. Rebolledo. 2010. Landslides induced by the April 2007 Aysén fjord earthquake, Chilean Patagonia. *Landslides*, 7(4), 483-492. DOI: 10.1007/s10346-010-0203-2

Slingerland, R.L., and B. Voight. 1979. Occurrences, properties, and predictive models of landslide-generated water waves. *Developments in Geotechnical Engineering* 14B, Rockslides and avalanches 2, Engineering Sites, B. Voight, ed. Elsevier Scientific Publishing, Amsterdam, 317-397.